

Research Paper

Novel Self-assembled Organic Nanoprobe for Molecular Imaging and Treatment of Gram-positive Bacterial Infection

Tang Gao¹, Hongliang Zeng², Huan Xu³, Feng Gao³, Wei Li³, Shengwang Zhang³, Yi Liu¹, Guifang Luo², Mingdan Li², Dejian Jiang², Zhigao Chen², Yong Wu³, Wei Wang³, Wenbin Zeng^{1,✉}

1. Xiangya School of Pharmaceutical Sciences, Central South University, Changsha 410013, China.
2. Hunan Provincial Research Center for Safety Evaluation of Drugs, Liuyang National Economic and Technical Development Zone 410331, China.
3. The Third Xiangya Hospital, Central South University.

✉ Corresponding author: Prof Dr Wenbin Zeng, Tel(Fax): 0086-731-82650459; E-mail address: wbzeng@hotmail.com (W. Zeng)

© Ivyspring International Publisher. This is an open access article distributed under the terms of the Creative Commons Attribution (CC BY-NC) license (<https://creativecommons.org/licenses/by-nc/4.0/>). See <http://ivyspring.com/terms> for full terms and conditions.

Received: 2017.08.25; Accepted: 2017.12.27; Published: 2018.02.14

Abstract

Background: Increasing bacterial infections as well as a rise in bacterial resistance call for the development of novel and safe antimicrobial agents without inducing bacterial resistance. Nanoparticles (NPs) present some advantages in treating bacterial infections and provide an alternative strategy to discover new antibiotics. Here, we report the development of novel self-assembled fluorescent organic nanoparticles (**FONs**) with excellent antibacterial efficacy and good biocompatibility.

Methods: Self-assembly of 1-(12-(pyridin-1-ium-1-yl)dodecyl)-4-(1,4,5-triphenyl-1H-imidazol-2-yl)pyridin-1-ium (**TPIP**) in aqueous solution was investigated using dynamic light scattering (DLS) and transmission electron microscopy (TEM). The bacteria were imaged under a laser scanning confocal microscope. We evaluated the antibacterial efficacy of **TPIP-FONs** *in vitro* using sugar plate test. The antimicrobial mechanism was explored by SEM. The biocompatibility of the nanoparticles was examined using cytotoxicity test, hemolysis assay, and histological staining. We further tested the antibacterial efficacy of **TPIP-FONs** *in vivo* using the *S. aureus*-infected rats.

Results: In aqueous solution, **TPIP** could self-assemble into nanoparticles (**TPIP-FONs**) with characteristic aggregation-induced emission (AIE). **TPIP-FONs** could simultaneously image gram-positive bacteria without the washing process. *In vitro* antimicrobial activity suggested that **TPIP-FONs** had excellent antibacterial activity against *S. aureus* (MIC = 2.0 $\mu\text{g mL}^{-1}$). Furthermore, **TPIP-FONs** exhibited intrinsic biocompatibility with mammalian cells, in particular, red blood cells. *In vivo* studies further demonstrated that **TPIP-FONs** had excellent antibacterial efficacy and significantly reduced bacterial load in the infectious sites.

Conclusion: The integrated design of bacterial imaging and antibacterial functions in the self-assembled small molecules provides a promising strategy for the development of novel antimicrobial nanomaterials.

Key words: antibacterial materials, self-assembly, aggregation-induced emission, bacterial imaging, antimicrobial activity.

Introduction

Despite the availability of antibiotics, bacterial infections remain one of the major causes of deaths worldwide. This is due to the emergence of bacterial

resistance which has become a global health challenge threatening public health [1]. In the United States alone, more than 2 million people suffer from

antibiotic-resistant infections each year, and at least 23,000 people die as a result of these infections [2]. The bacterial resistance can be attributed to various mechanisms, such as activation of antibiotic efflux pumps, inactivation of antibiotic degradation enzymes, decreased antibiotic permeation and formation of biofilm [3]. To treat drug-resistant bacterial infections, numerous antimicrobial materials have been developed recently, such as cationic polymers [4-7], antimicrobial peptides [8-13], silver nanoparticles (AgNPs) [14-19], and metal-containing NPs [20-22]. Among these, cationic polymers have some beneficial properties, such as broad-spectrum antibacterial features and the ability for easy functionalization. However, they can also cause a certain degree of hemolysis *in vivo* and exert some cytotoxicity to human cells inhibiting their application as an antibacterial agent [23, 24]. Although antimicrobial peptides (AMP) are efficient, their application is still restricted because of the high cost, limited stability (when composed of L-amino acids), poor photolytic stability, and poorly-studied toxicology and pharmacokinetics [25, 26].

AgNPs are popular antimicrobial inorganic NPs and show a higher antimicrobial activity against multidrug resistant (MDR) bacteria [27, 28]. However, the toxic side effects of AgNPs on humans, like spasms, gastrointestinal disorders, and even death, limit their therapeutic application [17, 29]. Moreover, studies indicated that AgNPs could cause potential immunotoxicity [30, 31]. Other metal-containing NPs also have limitations for antibacterial treatments *in vivo* due to the accumulation of toxicity. Therefore, it is critical to design and synthesize innovative antibacterial materials with efficient activity and decent biocompatibility for clinical treatments.

Besides countering the issue of drug-resistance, developing a new method for quick bacterial detection is also important for microbial infection treatment and controlling the spread of disease [32, 33]. Gram staining has been the standard method to differentiate bacterial species into two large groups, gram-positive and gram-negative [34]. However, this method is prone to generate false positive results [35]. Other methods, such as enzyme-linked immunosorbent assay (ELISA) [36, 37] and polymerase chain reaction (PCR) [38-39] with high sensitivity and reproducibility, have been reported for microbial detection. Nevertheless, these technologies require lengthy and laborious procedures [40] thereby delaying the critical diagnosis and response to infectious emergencies. Recently, fluorescence assay has been demonstrated as an effective method to detect bacteria in different biological environments [41-47]. For example, antibiotics (vancomycin and

daptomycin)-modified fluorophores and nanoparticles are synthesized for targeted bacterial detection [12, 41, 48-50]. Multidrug resistant bacteria, however, would not be detected by the antibiotic-modified probes thus leading to false negative results. Furthermore, the administration of sub-lethal doses of antibiotics may promote unexpected antimicrobial resistance.[51]

NPs hold great potential for both antibacterial application and rapid detection of pathogens due to their unique physicochemical properties that feature a large surface area to volume ratio and a versatile surface chemistry [52-55]. Specifically, the large surface area of nanomaterials can enhance their interactions with microbes. Also, NPs are believed to be more effective and less likely to induce resistance in most drug-resistant cases, since their antimicrobial properties involve direct contact with the bacterial cell wall, instead of penetrating into the cell, making most bacterial antibiotic-resistant mechanisms irrelevant [56-59]. Therefore, the nano-antibacterial agents may be less prone to induce resistance in bacteria than traditional antibiotics.

Molecular self-assembly is a spontaneous association of individual components into well-ordered structures assisted by non-covalent interactions including electrostatic interaction, hydrogen bonding, π - π interaction, charge-transfer interactions, and hydrophobic effect [60, 61]. Among the reported self-assembled nano-materials, small molecule self-assembled nanomaterials have received much attention for their photo-stability, biocompatibility, diversity, and flexibility in molecular design [62-64]. However, to the best of our knowledge, the usage of small molecule self-assembled nanomaterials in diagnostic and therapeutic platforms against microbial infections is still lacking.

Recently, based on tetraphenyl imidazole-cored molecular rotors, our group developed a novel series of AIEgens with good photo-stability, high water solubility, and good biocompatibility. It was reported that tetraphenyl imidazole derivatives could self-assemble into nanoparticles for chemical sensing or imaging of gram-positive bacterial strains [65, 66]. In this study, inspired by the antimicrobial activity of the imidazole moiety [67-69] and the excellent antibacterial effect of quaternary ammonium compounds [70-72], we designed a cationic bola-type small molecule by combining tetraphenyl imidazole core with quaternary ammonium group (TPIP) for fast microbial detection and bacterial infection treatment. TPIP is composed of three components (**Scheme 1**): (1) the substituted imidazole is used as the AIEgen with antibacterial activity, (2) the alkyl

chain can tune the spatial positioning of the positive charge in molecules and reduce the toxicity of small cationic molecules, and (3) the pyridinium salt group serving as the hydrophilic terminal group has an antimicrobial effect. This bola-type molecule can self-assemble into nanoparticles (**TPIP-FONs**) in aqueous solution without fluorescence, while it emits intense green fluorescence after bonding with gram-positive bacteria. The *in vitro* antimicrobial activity studies revealed that **TPIP-FONs** have excellent antibacterial activity. The low cytotoxicity and negligible hemolysis activity of **TPIP-FONs** allowed us to treat bacterial infections *in vivo*. To the best of our knowledge, this is the first report on the small molecule self-assembled nanomaterials enabling bacterial imaging and antibacterial action.

Experimental section

Materials and instruments

Vitamin B₁, benzaldehyde, aniline (99.5%), and 1, 12-dibromo dodecane (98%) were purchased from Energy Chemical Co., Ltd (China). Two compounds (4-pyridine carboxaldehyde (98%) and pyridine) were obtained from Sinopharm Chemical Reagent Co., Ltd (China). Mannitol Salt Agar was purchased from Beijing Land Bridge Technology Co., Ltd (China). All bacterial strains were acquired from American Type Culture Collection (ATCC), USA. Dulbecco's Modified Eagle's Medium, fetal bovine serum, penicillin G (100 U mL⁻¹), streptomycin (100 U mL⁻¹) and 0.25% trypsin solution were purchased from Gibco (USA). AT-II cells and L02 cells were from the Cell Bank of Chinese Academy of Sciences. Ultrapure water was obtained by using a Millipore water

purification system (Merck Millipore, Germany). Other chemical reagents and solvents were purchased from commercial chemical suppliers and used without further purification.

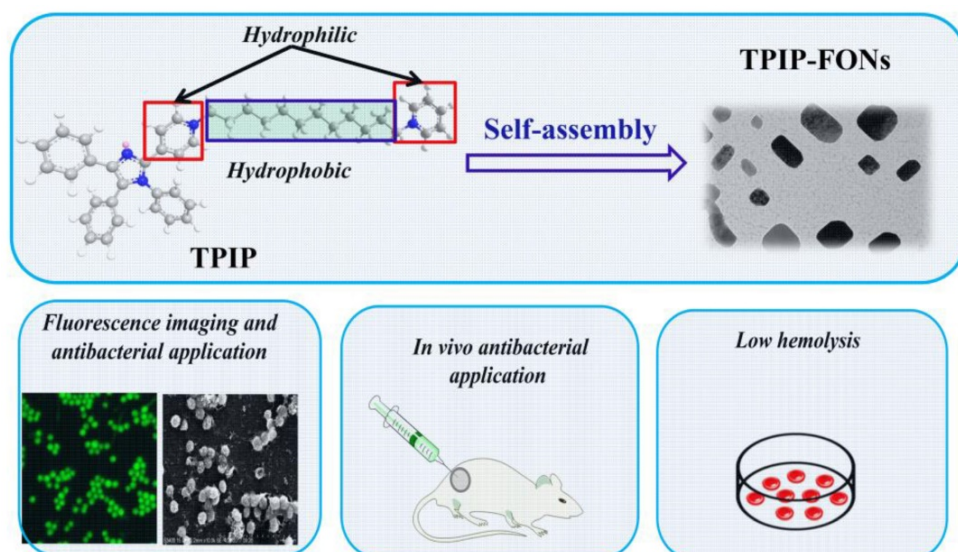
UV-vis absorption spectra were performed on a UV-2550 scanning spectrophotometer (Shimadzu, Japan). Fluorescent spectra were recorded on a Shimadzu RF-5301 equipped with a 1 cm quartz cell. Dynamic light scattering measurements were performed at 25 °C on Zestier Nano ZS (Malvern Instruments Ltd, UK). The morphology of **TPIP-FONs** was characterized by JEM-2100 transmission electron microscope with an accelerating voltage of 200 kV. The morphology of bacteria was characterized by S-3400N scanning electron microscope (Hitachi, Japan) with an accelerating voltage of 15 kV. ¹H NMR and ¹³C NMR were measured on a Bruker AVII-400 MHz or 500 MHz spectrometers with chemical shifts reported in ppm (in DMSO-d₆ or CDCl₃, TMS as internal standard). HRMS was obtained on an Orbitrap Velos Pro LC-MS spectrometer (Thermo Scientific, American).

Preparation of TPIP-FONs

A stock solution of **TPIP** (1×10⁻³ M) was prepared from dimethyl sulfoxides. Thirty microliters of this solution was added to phosphate buffer (3 mL) maintained at pH 7.4, and the solution (10 μM) was kept at room temperature. Nanoparticles formation was confirmed by DLS and TEM analyses for which the solution was dropped casting on freshly cleaved mica surface or carbon-coated copper grid (400 mesh), respectively, after drying under vacuum.

Bacterial cultures and staining assays

A single colony of bacteria *S. aureus*, *P. aeruginosa*, *S. epidermidis*, *E. faecalis*, *Streptococcus*, *A. baumannii*, *K. pneumoniae*, or *E. coli* on solid Luria-Bertani (LB) medium was transferred to 10 mL of liquid culture medium and grown at 37 °C for 12 h with 180 rpm rotation. The concentration of bacteria was determined by measuring optical density at 600 nm



Scheme 1. Schematics of the structure of **TPIP** and its self-assembled nanoparticles (**TPIP-FONs**) with low hemolysis and the antibacterial application *in vitro* and *in vivo*.

(OD₆₀₀). Subsequently, 10⁹ colony forming unit (CFU) (OD₆₀₀ = 10⁹ CFU mL⁻¹) of bacteria was transferred to a 1.5 mL EP tube. Bacteria were harvested by centrifuging at 5000 rpm for 3 min. After removal of the supernatant, 500 µL **TIPI-FONs** were added to the EP tube with PBS, making the final concentration of **TIPI-FONs** to 20×10⁻⁶ M). After vortexing to disperse, the bacteria were incubated at room temperature for 10 min. *S. aureus* samples were diluted into various concentrations (from 3×10⁷ to 3×10⁸ CFU mL⁻¹) by using sterile saline, then 10 µL **TIPI-FONs** (50×10⁻⁶ M) was added to the 90 µL bacterial solutions, and incubated for 10 min. The fluorescence of solutions was recorded by fluorescence spectrophotometer.

Bacterial imaging

For fluorescence images, 10 µL of the stained bacterial solution was transferred to a glass slide and covered with a coverslip. The bacteria were imaged under a laser scanning confocal microscope using 400–440 nm excitation filter, and 490 nm long pass emission filters.

Kirby-Bauer antibiotic testing

The antibacterial efficacy of **TIPI-FONs** against *P. aeruginosa* or *S. aureus* was examined by Kirby-Bauer antibiotic testing. *P. aeruginosa* or *S. aureus* were diluted to approximately 1.0×10⁷ CFU mL⁻¹ with LB broth, and 50 µL of the bacterial suspension was inoculated on LB agar plates. The same disk containing different concentrations of **TIPI-FONs** solution was placed at the center of the plates, and cultured overnight at 37 °C. The diameter of the inhibition zone around the disk indicated the antibacterial activity.

Bacterial kinetic test: Bacteria in the log phase (1×10⁶ to 1×10⁷ CFU mL⁻¹) treated with different concentrations of **TIPI-FONs** were seeded in 96-well plates and cultured at 37 °C. During the culture process, the optical density at 600 nm of each well was monitored at different times.

Mannitol salt agar plate

The **TIPI-FONs** were mixed with mannitol salt agar medium at various concentrations (0–8 µg/mL). After the agar was cooled to room temperature, *S. aureus* suspensions (1×10⁵ to 1×10⁶ CFU mL⁻¹) were plated onto the above agar plates and incubated at 37 °C.

SEM characterization of bacteria

The bacteria in the logarithmic phase were treated with **TIPI-FONs** (2 µg/mL) for 2 h at 37 °C on a shaker bed at 200 rpm. Bacteria were collected by centrifugation at 5000 rpm for 3 min and washed with

sterile saline three times, fixed with 2.5% glutaraldehyde overnight at 4 °C and dehydrated with a sequential treatment of 50%, 70%, 85%, 90%, and 100% ethanol for 10 min each, and gold sputter-coated and observed by SEM.

Rats infection model: SD rats (200–230 g in weight) were purchased from the Hunan SJA Laboratory Animal Co. Ltd. (Hunan, China). All animal experimental procedures were performed according to the Guidelines for Animal Experimentation with the approval of the animal care committee of Central South University. To evaluate the *in vivo* antibacterial effect of **TIPI-FONs**, the *S. aureus*-infected rat model was developed. 200 µL of log-phase *S. aureus* cells (1×10⁹ CFU mL⁻¹) resuspended in sterile saline was injected into the rats. Two days after infection, 100 µL PBS with or without 200 µg/mL of **TIPI-FONs** was injected into the infectious site once a day. All rats were sacrificed after 2 days of treatment, and the infectious tissues and major organs (heart, liver, lung, kidney, and spleen) were processed for further analysis. To determine the number of bacteria, the infectious tissues were separated and homogenized in normal saline (0.5 mL). Aliquots of diluted (1:10, 1:100 and 1:1000) homogenized tissues were plated on mannitol salt agar plates (six plates per sample), and the number of colonies was counted.

Hemolysis assay

Hemolysis assay was conducted on RBCs. Human whole blood (2 mL) was donated by a healthy male volunteer. RBCs were centrifuged for five times and re-suspended using 10 mL PBS. 0.4 mL of different concentrations (0, 2, 4, 8, 16, 32, and 64 µg mL⁻¹) of **TIPI-FONs** dissolved in PBS were added to 0.1 mL of RBC solution. After incubation at 37 °C for 2 h, the supernatant was obtained by centrifugation at 4000 rpm for 5 min. The absorbance value of the supernatant was measured at 570 nm. RBCs in PBS and water were used as negative and positive controls, respectively. All samples were prepared in triplicates. The hemolysis percentage was calculated using the following formula:

$$\text{Hemolysis (\%)} = \frac{(\text{sample absorbance} - \text{negative control absorbance})}{(\text{positive control absorbance} - \text{negative control absorbance})} \times 100.$$

Histological staining

All SD rats were randomly divided into two groups. PBS-treated (control) group and **TIPI-FONs**-treated group (100 µL, 200 µg/mL) once daily. After administration for 2 d, major organs were separated and fixed in 4% formalin solution, then stained with hematoxylin and eosin (H&E), and examined using a digital microscope.

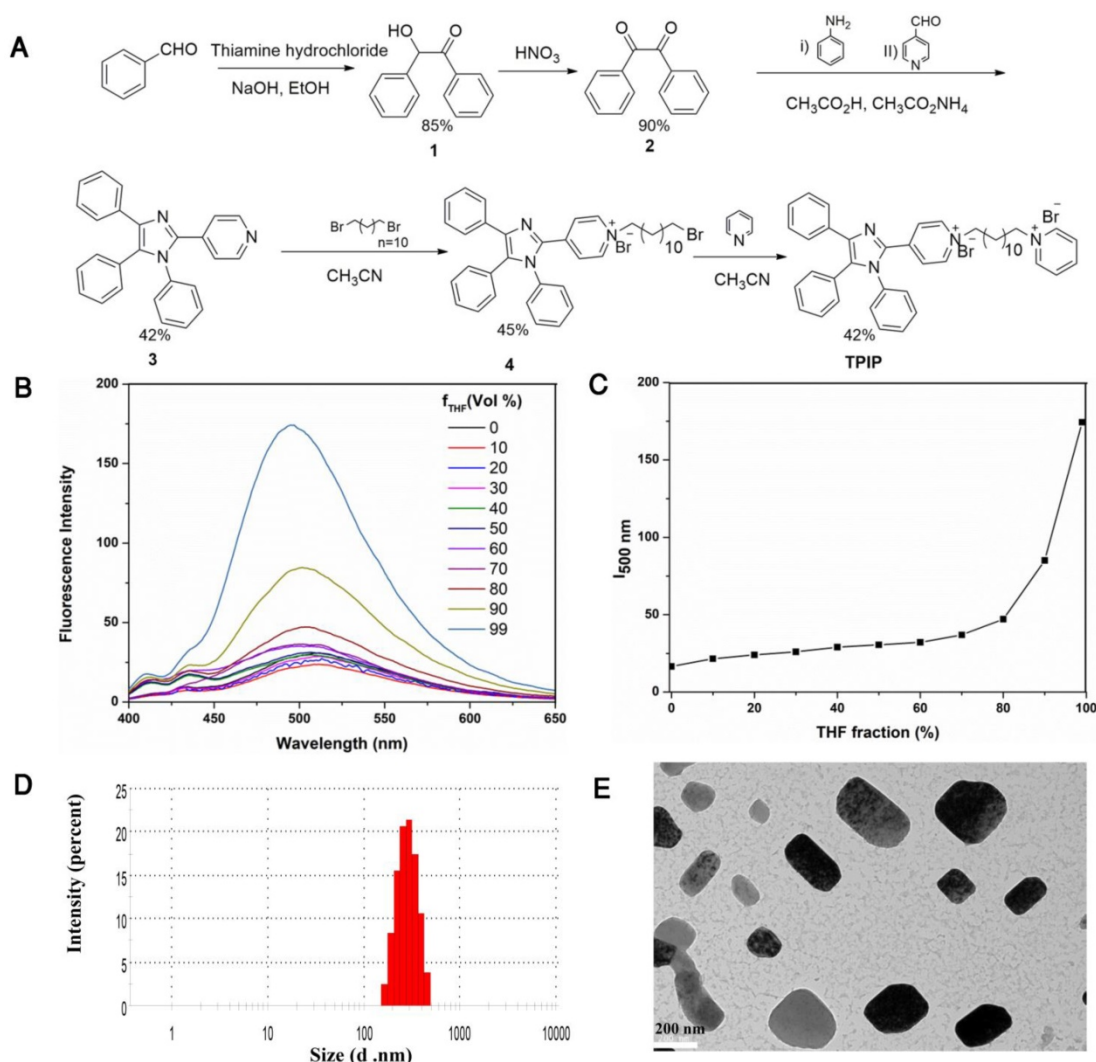


Figure 1. (a) Synthetic route of the bola-type molecule **TPiP**. (b) Fluorescent spectra of **TPiP** in THF-water mixtures with different THF fractions (f_w). (c) Plots of fluorescent intensity vs. THF fractions of **TPiP**. (d) DLS analysis of **TPiP** (10 μ M) assemblies obtained from water. (e) TEM analysis of **TPiP** (10 μ M) rectangular assemblies obtained from water.

Results and Discussion

Synthesis and characterization of **TPiP**

The bola-type molecule **TPiP** was synthesized as shown in **Figure 1a**. 2-hydroxy-1,2-diphenylmethane (compound **1**) was prepared by thiamine hydrochloride-mediated benzoin condensation reaction. Oxidation of compound **1** afforded the corresponding benzil (compound **2**). The tetraphenyl imidazole (compound **3**) was obtained by a one-pot two-steps multicomponent reaction of 4-pyridinecarboxaldehyde, primary aromatic amine, benzyl, and ammonium acetate. Compound **3** was reacted with 1, 12-dibromo dodecane to yield the intermediate **4**. The reaction of this intermediate with pyridine afforded the final **TPiP**. All compounds were characterized by NMR and MS.

To determine the characteristics of AIE, we used water and THF as the solvent and non-solvent. As

shown in **Figure 1b** and **Figure 1c**, **TPiP** showed weak fluorescence in aqueous solution and fluorescent quantum efficiency (ϕ_F) was 0.023. While the THF $f_w >$ was 80 (fraction by volume %), the emission of **TPiP** dramatically increased. This phenomenon resulted from the aggregations formed by **TPiP** which led to blocking the non-radiative relaxation pathways of its excited state, indicating that **TPiP** had a significant AIE effect. It is well known that some parameters, such as conductivity, surface tension, and fluorescence intensity of the solution significantly change around the critical aggregation concentration (CAC) [73, 74]. Therefore, CAC value of **TPiP** could be measured readily by the method of conductivity and fluorescence variation. When **TPiP** was dissolved in water, the conductivity (k), as a function of the concentration of **TPiP**, was measured to determine its CAC in water (**Figure S1a**). The conductivity increased linearly as the concentration of **TPiP**

increased up to 20 μM . However, when the concentration was higher than 20 μM , the plot was linear with a lower slope. The two linear segments in the curve and a sudden decrease of the slope indicated that the CAC value was approximately 20 μM . The fluorescence intensity at 500 nm versus the corresponding **TPIP** concentration is plotted in **Figure S1b**. The fluorescence of **TPIP** gradually arose with the increase in the concentration. Obviously, one inflection point appeared at around 20 μM (equal to the CAC obtained from the conductivity test), thus suggesting a change in the aggregation state.

Next, we investigated the photo-physical characteristics of **TPIP-FONs**. As shown in **Figure S2a**, the maximum absorption wavelength of **TPIP-FONs** was at 385 nm, and the **TPIP-FONs** solution exhibited weak fluorescence emission ($\Phi=0.023$) (**Figure S2b**). The aggregate of **TPIP** had weak emission because of its loosely packed characteristics with enough free volume to consume radiative energy by intramolecular rotation. Subsequently, the self-assembled behavior of **TPIP** in aqueous solution was investigated by using dynamic light scattering (DLS) and transmission electron microscopy (TEM). The DLS studies showed that the aggregates of **TPIP** (10 μM) had an average diameter of 313 nm (PDI: 0.296) and a broad size distribution (**Figure. 1d**) indicating that these aggregates may not be simple spherical assemblies. Furthermore, the TEM experiments were conducted to assist the visualization of nanostructures self-assembled from **TPIP** in water. **Figure 1e** shows a rectangular structure of the aggregates and the average diameter of 100-300 nm for **TPIP-FONs**. This aggregate of **TPIP** had weak emission owing to its loosely packed characteristics and still had enough free volume to consume radiative energy by the intramolecular rotation.

Detection of bacteria

Given that **TPIP** has two quaternary ammonium structures with a positive charge while the cell wall of bacteria is negatively charged, we hypothesized that the electrostatic interaction between **TPIP** and the bacterial cells might alter the aggregation state of **TPIP** resulting in fluorescence emission, which could be used for the detection of bacteria. We, therefore, explored the fluorescence sensing ability of **TPIP-FONs** towards different species of bacteria. As shown in **Figure 2a**, the solution of **TPIP-FONs** exhibited weak fluorescence emission in the absence of bacteria while, upon addition of *S. aureus* cells, 8 times higher emission intensity was observed than that of **TPIP-FONs** alone. In sharp contrast, the fluorescence intensity of the solution was almost unchanged in the presence of the gram-negative *E. coli* cells. The selective “turn-on” detection was due to the strong interaction between **TPIP-FONs** and cell walls of gram-positive bacteria, *S. aureus*. Since the cell wall is mainly composed of negatively charged teichoic acids and a thick peptidoglycan layer, they are more likely to bind to quaternary ammonium compounds than gram-negative bacteria which is composed of a lipopolysaccharide-linked outer membrane [71, 75]. We then investigated the fluorescence response of **TPIP-FONs** to different concentrations of *S. aureus*. As shown in **Figure 2b**, upon addition of *S. aureus* cells, the fluorescence intensity constantly increased with the maximum emission wavelength blue-shifted from ~ 510 nm to ~ 490 nm. Importantly, the fluorescence intensity of **TPIP-FONs** showed an almost linear relationship between *S. aureus* concentrations in the range of 3×10^7 to 3×10^8 CFU mL^{-1} (**Figure 2c**). The limit of detection was determined to be 5.2×10^5 CFU mL^{-1} which was calculated by $3\sigma/k$ (σ is the standard deviation of blank measurements, $n=11$, and k is the slope of the linear equation). We performed additional experiments and detected the bacteria from

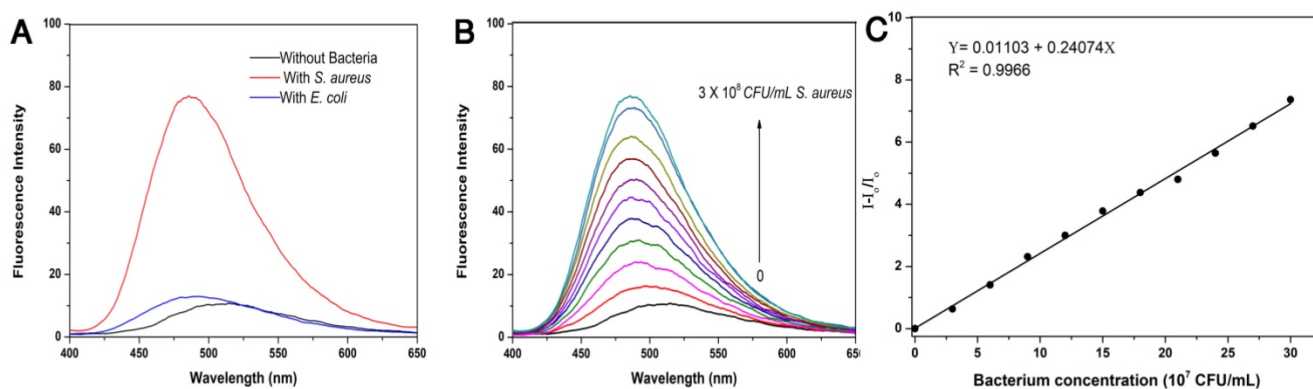


Figure 2. (a) Fluorescence emission spectra of **TPIP-FONs** (5 μM) with/without 3×10^8 CFU mL^{-1} of *S. aureus* or *E. coli*. Excitation wavelength: 380 nm. (b) Fluorescence intensity of **TPIP-FONs** aqueous solution upon addition of varying amounts of *S. aureus* cells. (c) Fluorescence intensity ($I-I_0/I_0$) at 490 nm against concentrations of *S. aureus* cells.

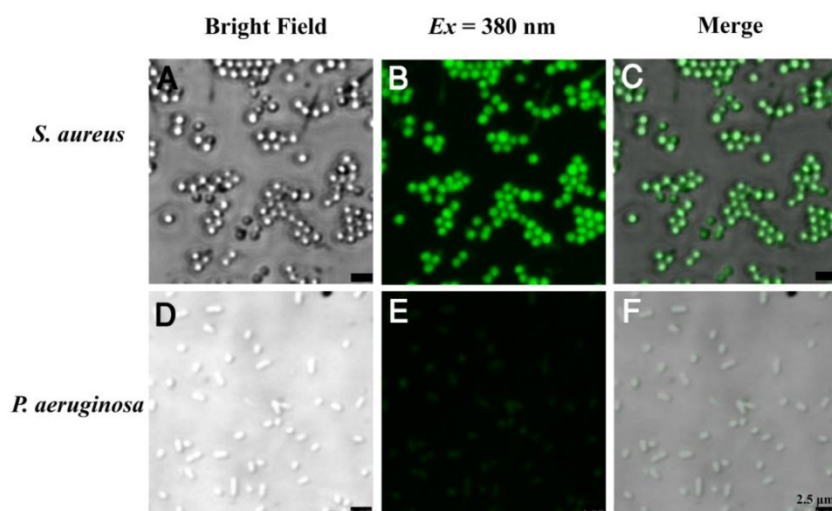


Figure 3. Confocal fluorescence images of (a-c) *S. aureus* and (d-f) *P. aeruginosa* bacteria after incubation with 5 μM **TIIP-FONs** for 10 min and visualized under bright field; excitation at 380 nm, and the overlay.

0 to 3×10^7 CFU mL^{-1} . As shown in **Figure S3**, the fluorescence intensity of **TIIP-FONs** showed an almost linear relationship between *S. aureus* concentrations in the range of 9×10^5 to 3×10^7 CFU mL^{-1} . The R^2 presented a better linear relationship in the wide range as compared to the short range. The fluorescence “turn-on” detection of bacteria with good accuracy and large linear relationship region enabled its further application for detecting bacteria in the clinic.

The bola-type amphiphilic molecule **TIIP** contained positively charged amines and the long alkyl chain signifying hydrophilicity and hydrophobicity, respectively. At the concentrations below CAC, **TIIP-FONs** showed very weak fluorescence in aqueous solution, and were able to turn on their fluorescence after binding with gram-positive bacteria. Due to their AIE characteristics, the unbound molecules of **TIIP** exhibited faint fluorescence and only those bounded to bacteria lit up. This unique property provides an opportunity for the direct identification of bacteria without washing process. We next applied **TIIP-FONs** for imaging the bacteria. As shown in **Figure 3**, **TIIP-FONs** could be used to selectively image the gram-positive *S. aureus* bacteria while the gram-negative *P. aeruginosa* bacteria were rarely stained. Furthermore, we also used **TIIP-FONs** for imaging three additional gram-positive (*S. epidermidis*, *E. faecalis*, and *Streptococcus*) and three gram-negative bacteria (*A. baumannii*, *K. pneumoniae*, and *E. coli*). The results shown in **Figure S4** and **Figure S5** further confirmed that **TIIP-FONs** specifically stained gram-positive bacteria. This selective imaging of gram-positive bacteria was due to the different cell wall structures of gram-positive and negative bacteria.

Antimicrobial activity of **TIIP-FONs** in vitro

Considering the excellent antibacterial activity of quaternary ammonium and imidazole compounds, we hypothesized that **TIIP-FONs** has potent antibacterial activity. To this end, the activity of **TIIP-FONs** was measured by agar diffusion test, a test of the antibiotic sensitivity of bacteria. **Figure 4a** and **Figure 4b** show the results of inhibition zones treated with different concentration of **TIIP-FONs** for *P. aeruginosa* and *S. aureus*, respectively. When the

concentration of **TIIP-FONs** was $8 \mu\text{g mL}^{-1}$, the inhibition zone for *P. aeruginosa* and *S. aureus* was 0.6 cm and 0.9 cm, respectively. The concentration of **TIIP-FONs** was as low as $32 \mu\text{g mL}^{-1}$ showed significant antibacterial activity against *S. aureus* (The inhibition zone close to 1.25 cm). However, at the same concentration, the inhibition zone for *P. aeruginosa* was only 0.85 cm. Also, when the concentration of **TIIP-FONs** reached $128 \mu\text{g mL}^{-1}$, the antibacterial ring diameter of *S. aureus* (1.7 cm) was significantly larger than that of *P. aeruginosa* (1.3 cm). The results suggested that **TIIP-FONs** have better antibacterial activity against *S. aureus* than *P. aeruginosa* because gram-positive bacteria have more negative charge [77] resulting in the stronger interaction with **TIIP-FONs** than gram-negative bacteria.

To quantitatively evaluate the antibacterial activity of **TIIP-FONs**, the growth kinetics of *P. aeruginosa* and *S. aureus* in liquid media were studied. Bacterial growth was monitored by measuring the optical density at 600 nm (OD_{600} is recognized as the characteristic peak for determining the bacterial number) at different incubation times. The results showed that **TIIP-FONs** could inhibit the growth of *S. aureus* within 24 h at a concentration of $2 \mu\text{g mL}^{-1}$ (**Figure 4c**). In contrast, even at a concentration of $32 \mu\text{g mL}^{-1}$, the growth of *P. aeruginosa* was not inhibited for 24 h (**Figure 4d**). To further explore its antibacterial activity, we also measured the growth kinetics of *E. coli* and *C. albicans*. In case of *E. coli*, when the concentration of **TIIP-FONs** reached $8 \mu\text{g mL}^{-1}$, the bacterial growth was significantly inhibited within 24 h (**Figure S6**). The growth of *C. albicans* was also completely inhibited by $2 \mu\text{g mL}^{-1}$ **TIIP-FONs** (**Figure S7**). The MICs (minimum inhibitory concentration) of **TIIP-FONs** against different

bacteria are shown in Table S1. The results further confirmed that TPIP-FONs exhibited an excellent antibacterial activity which could be observed with

naked eyes. The agar plate experiments for *S. aureus* were also carried out (Figure 4e). Compared to the group without treatment, 0.5 $\mu\text{g mL}^{-1}$ of TPIP-FONs showed a slight inhibitory effect on *S. aureus*. When the concentration of TPIP-FONs was increased to 2 $\mu\text{g mL}^{-1}$, the number of *S. aureus* colonies significantly decreased, but some bacteria were still alive. In the presence of 8 $\mu\text{g mL}^{-1}$ TPIP-FONs, *S. aureus* was killed effectively and almost no colony formed on the plate. These results proved the excellent antibacterial efficacy of TPIP-FONs against *S. aureus*.

Antimicrobial mechanism

Having demonstrated the excellent antimicrobial activity of TPIP-FONs, we further investigated their antibacterial mechanism. To this end, we tested the morphological changes of *E. coli* and *S. aureus* before or after incubation with TPIP-FONs (2 $\mu\text{g mL}^{-1}$) by SEM observations. As shown in Figure 5a and Figure 5c, both *E. coli* and *S. aureus* without TPIP-FONs

treatment exhibited integrity of the membrane structure with a smooth surface. After incubation with TPIP-FONs for 2 h, the cell walls of *S. aureus* became wrinkled and damaged, and the leakage of intracellular contents could be observed (Figure 5d). Moreover, some outer membrane vesicles (OMVs) formed on the cell membrane after incubation with TPIP-FONs, which could be ascribed to the instability of cell membranes. [79] The formation of OMVs was also observed in bacteria treated with cationic antibiotics such as polymyxin and gentamicin.

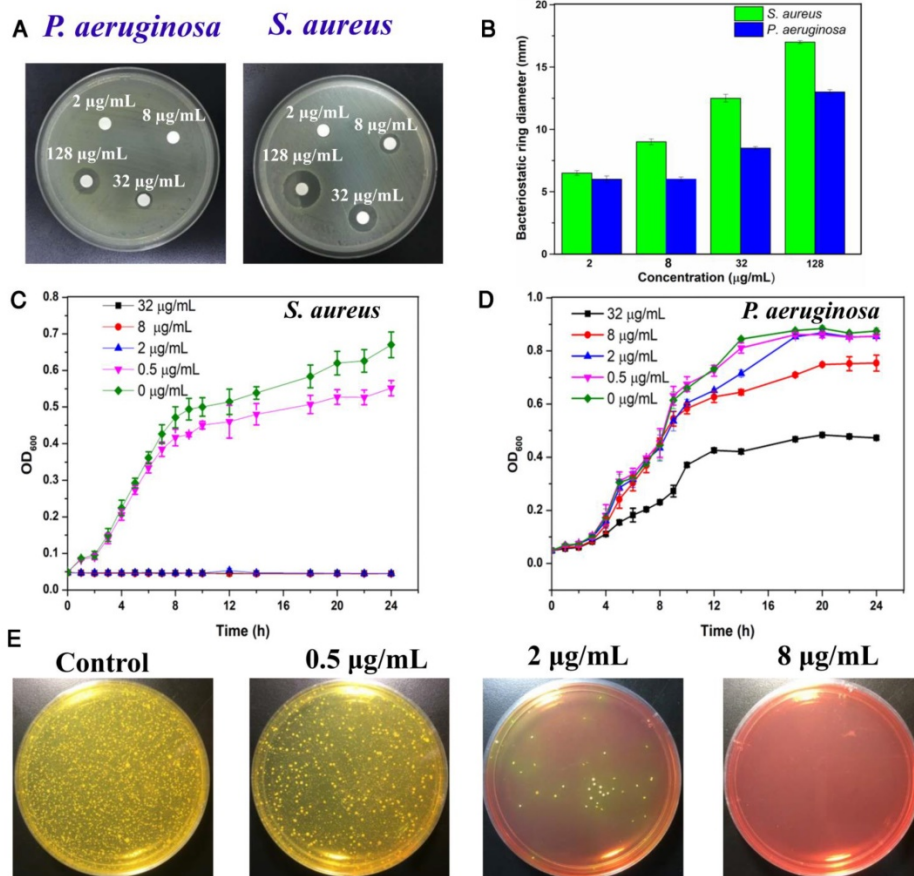


Figure 4. (a) Inhibition zones of different concentrations of TPIP against *P. aeruginosa* and *S. aureus*. (b) The bacteriostatic ring diameters of different samples. (c) Inhibitory effect of different concentrations of TPIP on the growth of *S. aureus* as a function of incubation time. (d) Inhibitory effect of different concentrations of TPIP on the growth of *P. aeruginosa* as a function of incubation time. (e) Photographs of the agar plates of *S. aureus* after treatments with different concentrations of TPIP.

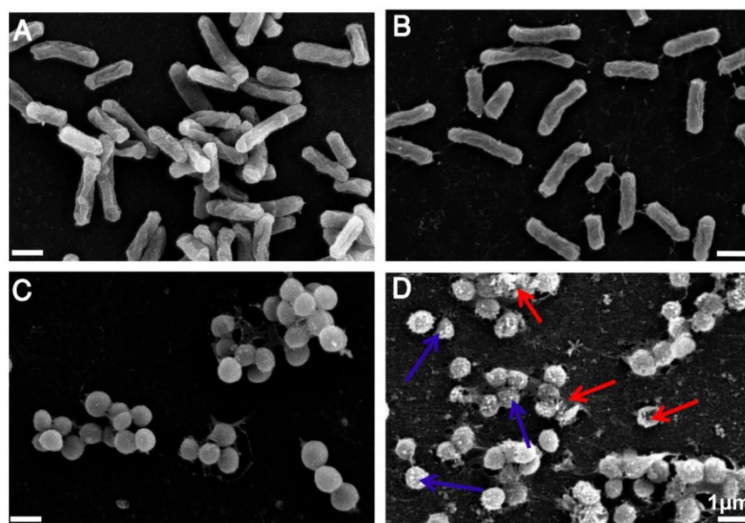


Figure 5. (a) SEM images of *E. coli* without treatment of TPIP-FONs. (b) SEM images of *E. coli* with the treatment of 2 $\mu\text{g mL}^{-1}$ TPIP-FONs for 2 h. (c) SEM images of *S. aureus* without treatment of TPIP-FONs. (d) SEM images of *S. aureus* with the treatment of 2 $\mu\text{g mL}^{-1}$ TPIP-FONs for 2 h. Red arrows indicate the damage of bacterial cells. Blue arrows show the formation of outer membrane vesicles (OMVs) on the surface of bacteria cells.

[78, 79] In contrast, after the treatment of *E. coli* cells with TPIP-FONs at the same concentration, almost no morphological changes could be observed between treated and untreated cells (Figure 5a and 5b). These results indicated that TPIP-FONs could exhibit better antibacterial activity against *S. aureus* than *E. coli*. Normally, gram-positive bacteria have a single phospholipid membrane and a thicker cell wall composed of peptidoglycan, whereas gram-negative bacteria are encapsulated by two cell membranes and fairly thin peptidoglycan. Therefore, quaternary ammonium compounds and other membrane-targeting antiseptics tend to exhibit decreased activity against gram-negative species. [70] The ability of bacterial cell wall disruption enables TPIP-FONs to effectively combat bacterial drug resistance, making it difficult for bacteria to develop drug tolerance. We believe that the possible antimicrobial mechanism of TPIP-FONs is through the following sequential events. First, electrostatic interactions between the positively-charged

pyridinium head and the negatively-charged teichoic acids are followed by the permeation of alkyl chain of TPIP into the intramembrane region of gram-positive bacteria. Subsequently, increase of microbial cell membrane permeability, osmotic damage, and leakage of cytoplasmic material out of the cell eventually lead to cell death.

In vivo antimicrobial activity

We further evaluated the antibacterial efficacy of TPIP-FONs *in vivo* using the *S. aureus*-infected rats. The rats were divided into two groups, the PBS-treated group (control) and the TPIP-FONs-treated group. The drugs were injected once a day. During the therapy, no obvious change in the activity and body weight was observed. Obvious skin infection could be observed in the PBS-treated group (Figure 6b and Figure S8a), whereas the TPIP-treated group exhibited slight skin infection after the 4th day of treatment. We next examined the treatment effect by hematoxylin and eosin staining (H&E

staining). As shown in Figure 6c, a large number of inflammatory cells and fragmentary epidermal layer appeared on the skin tissue of infection sites in the control groups, while fewer inflammatory cells were observed on the skin tissue of rats treated with TPIP-FONs for 2 days (Figure 6d). Therapeutic efficacy was further evaluated by enumerating the bacterial counts in the mannitol high salt agar medium for the homogenized tissue dispersions from the infectious site (Figure 6e). The number of *S. aureus* colonies from the infected tissues was 4.78×10^6 CFU g⁻¹ after treatment with PBS. Tissues of rats treated with TPIP-FONs showed a bacterial burden of 7.2×10^5 CFU g⁻¹, which was a significant reduction (with 85% bactericidal efficacy) compared to the control group. Thus, it can be concluded that TPIP-FONs exhibited an excellent antibacterial effect *in vivo*.

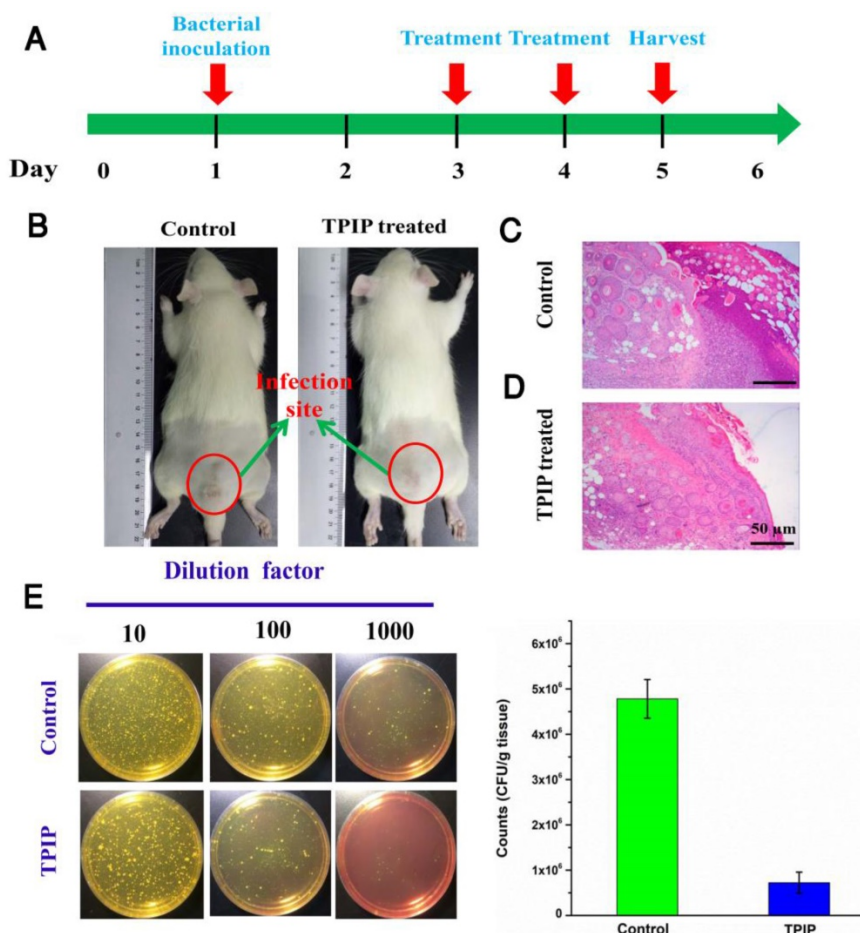


Figure 6. (a) The schematic diagram of *S. aureus*-infected rat model and the therapeutic evaluation TPIP-FONs. (b) Photographs of *S. aureus*-infected rat treated with PBS (control) or TPIP-FONs solution. (c & d) Histological images of the skin from the control group and from the group treated with TPIP-FONs. (e) Photographs of the bacterial colonies and corresponding statistical histogram derived from the homogenized tissue dispersion of the infected sites injected with PBS and TPIP-FONs. The tissue dispersions were diluted (10, 100 and 1000 times) and plated on mannitol high salt agar medium at 37 °C for 12 hours.

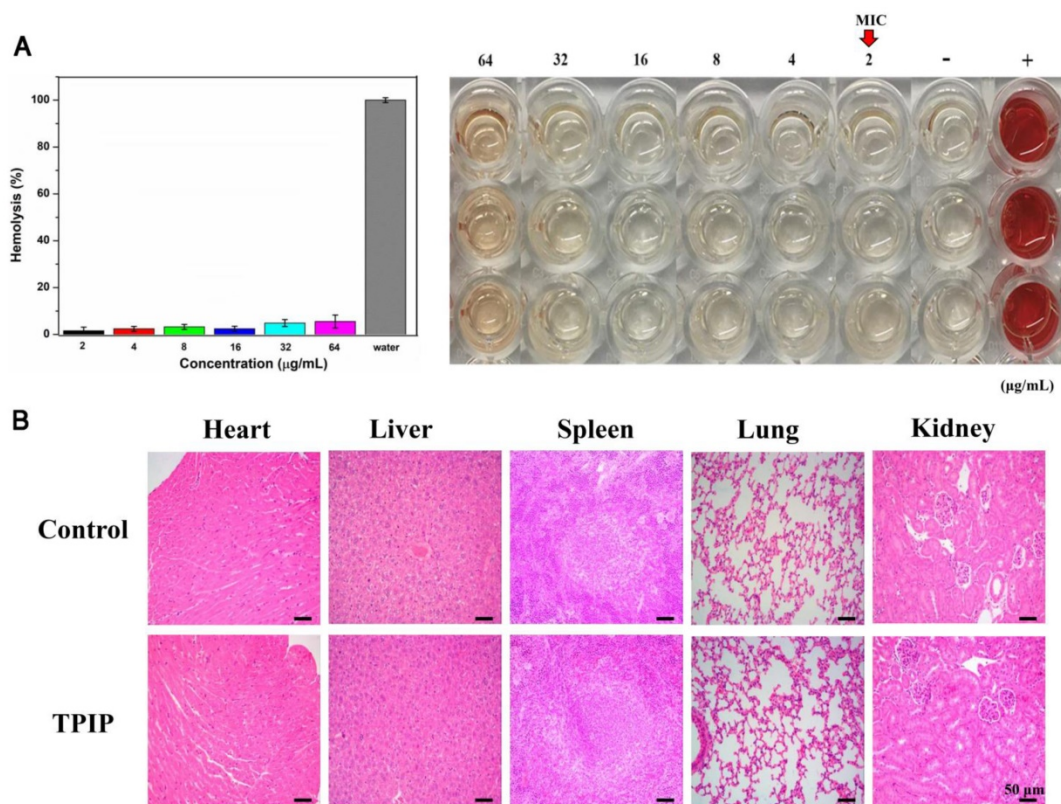


Figure 7. (a) Hemolysis assay of **TPIP-FONs** at several concentrations on human RBCs for 30 min at 37 °C. The mixture was centrifuged to detect the cell-free hemoglobin in the supernatant. RBCs incubated with PBS and water were used as negative (-) and positive (+) controls, respectively. (b) Histological evaluation of different organs (heart, liver, spleen, lung, and kidney) from rats treated with PBS and **TPIP-FONs**.

Biological safety of TPIP-FONs

For therapeutic use of antibacterial drugs, it is important to ensure that they have significant activity against bacteria but exhibit low toxicity to mammalian cells, in particular, red blood cells (RBCs). [29, 80] To determine the cytocompatibility of **TPIP-FONs**, the cytotoxicity of **TPIP-FONs** to AT II (normal lung cells) and L02 (normal liver cells) cells was evaluated by the MTT assay. As shown in **Figure S9**, the cell viability of AT-II or L02 cells was over 80% at a concentration of up to 64 µg mL⁻¹, which was much higher than the MICs for *S. aureus*. The hemolytic activity of **TPIP-FONs** against red blood cells was also tested. In this experiment, RBCs in PBS and water solution were used as negative and positive controls, respectively. At a concentration of up to 64 µg mL⁻¹, no obvious hemolytic activity (hemolysis rate: 5.22%) of **TPIP-FONs** was observed (**Figure 7a**). The results demonstrated that **TPIP-FONs** had good biocompatibility with mammalian cells and human RBCs. Finally, the *in vivo* toxicity of **TPIP-FONs** was also evaluated. The main organs of rats including the heart, lung, liver, kidney, and spleen were collected and examined histopathologically. **TPIP-FONs** treatment showed negligible effects on the normal

anatomical structures of various organs compared to untreated controls (**Figure 7b**), demonstrating the safety of **TPIP-FONs** as a potential therapeutic agent.

Conclusion

In summary, we constructed, for the first time, a bola type of molecule **TPIP** with AIE property, high water solubility, and antibacterial effect. **TPIP** can self-assemble into a rectangular structure of nanoparticles in aqueous solution. Due to the superior optical properties, **TPIP-FONs** can recognize and image gram-positive bacteria without any washing procedure. The imaging mechanism can be explained by the synergistic electrostatic and hydrophobic interactions between the negatively charged gram-positive bacterial cell wall and the self-assembled nanoparticles of **TPIP-FONs**. SEM observations indicate that the nanoparticles cause disruption of the cytoplasmic membrane and leakage of cytoplasm. *In vitro* antimicrobial activity suggests that **TPIP-FONs** have excellent antibacterial activity against *S. aureus*. Most importantly, **TPIP-FONs** exhibit intrinsic biocompatibility towards mammalian RBCs. Because of the low cytotoxicity and negligible hemolysis activity, **TPIP-FONs** can be used as an antibacterial agent *in vivo*. The integrated design of bimodal

bacterial imaging with the antibacterial function of the self-assembled small molecules represents a novel strategy towards the construction of next-generation “theranostics” system in the field of bacterial prevention/treatment. Thus, TPIP-FONs exert a futuristic impact on the development of self-assembled small molecule antimicrobial nanomaterials for biomedical applications.

Abbreviations

DLS: Dynamic Light Scattering; TEM: Transmission Electron Microscopy; AIE: Aggregation-Induced Emission; MIC: Minimum Inhibitory Concentration; RBCs: Red blood cells; CAC: Critical Aggregation Concentration; OMVs: outer membrane vesicles.

Acknowledgements

This work was supported by the National Natural Science Foundation of China (81671756 and 81741134), Key Research Project of Science and Technology Foundation of Hunan Province (2017SK2090). We thank Varadha Balaji Venkadakrishnan for their efforts for language improvement. The authors also acknowledge the NMR measurements by the Modern Analysis and Testing Center of CSU.

Supplementary Material

Supplementary figures.

<http://www.thno.org/v08p1911s1.pdf>

Competing Interests

The authors have declared that no competing interest exists.

References

- Laxminarayan R, Matsoso P, Pant S, Brower C, Røttingen J-A, Klugman K, et al. Access to effective antimicrobials: a worldwide challenge. *Lancet*. 2016; 387: 168-175.
- Control CfD. Prevention. Antibiotic resistance threats in the United States, 2013: Centres for Disease Control and Prevention. US Department of Health and Human Services; 2013.
- Khameneh B, Diab R, Ghazvini K, Bazzaz BSF. Breakthroughs in bacterial resistance mechanisms and the potential ways to combat them. *Microb Pathogen*. 2016; 95: 32-42.
- Ng VWL, Ke X, Lee AL, Hedrick JL, Yang YY. Synergistic codelivery of membrane-disrupting polymers with commercial antibiotics against highly ippportunistic bacteria. *Adv Mater*. 2013; 25: 6730-6.
- Li P, Zhou C, Rayatpisheh S, Ye K, Poon YF, Hammond PT, et al. Cationic peptidopolysaccharides show excellent broad-spectrum antimicrobial activities and high selectivity. *Adv Mater*. 2012; 24: 4130-7.
- Chen Z, Yuan H, Liang H. Synthesis of multifunctional cationic poly(p-phenylenevinylene) for selectively killing bacteria and lysosome-specific imaging. *ACS Appl Mater Interfaces*. 2017; 9: 9260-4.
- Li P, Poon YF, Li W, Zhu H-Y, Yeap SH, Cao Y, et al. A polycationic antimicrobial and biocompatible hydrogel with microbe membrane suctioning ability. *Nat Mater*. 2011; 10: 149-56.
- Liu L, Xu K, Wang H, Tan PJ, Fan W, Venkatraman SS, et al. Self-assembled cationic peptide nanoparticles as an efficient antimicrobial agent. *Nat Nanotechnol*. 2009; 4: 457-63.
- Salick DA, Pochan DJ, Schneider JP. Design of an injectable β -hairpin peptide hydrogel that kills methicillin-resistant *S. aureus*. *Adv Mater*. 2009; 21: 4120-3.
- Some S, Ho S-M, Dua P, Hwang E, Shin YH, Yoo H, et al. Dual functions of highly potent graphene derivative-poly-L-lysine composites to inhibit bacteria and support human cells. *ACS Nano*. 2012; 6: 7151-61.
- Li NN, Li JZ, Liu P, Pranantyo D, Luo L, Chen JC, et al. An antimicrobial peptide with an aggregation-induced emission (AIE) luminogen for studying bacterial membrane interactions and antibacterial actions. *Chem Commun*. 2017; 53: 3315-8.
- Chen H, Zhang M, Li B, Chen D, Dong X, Wang Y, et al. Versatile antimicrobial peptide-based ZnO quantum dots for in vivo bacteria diagnosis and treatment with high specificity. *Biomaterials* 2015; 53: 532-44.
- Peschel A, Sahl H-G. The co-evolution of host cationic antimicrobial peptides and microbial resistance. *Nat Rev Microbiol*. 2006; 4: 529-36.
- Verma VC, Kharwar RN, Gange AC. Biosynthesis of antimicrobial silver nanoparticles by the endophytic fungus *Aspergillus clavatus*. *Nanomedicine*. 2010; 5: 33-40.
- Dai X, Guo Q, Zhao Y, Zhang P, Zhang T, Zhang X, et al. Functional silver nanoparticle as a benign antimicrobial agent that eradicates antibiotic-resistant bacteria and promotes wound healing. *ACS Appl Mater Interfaces*. 2016; 8: 25798-807.
- Cao F, Ju E, Zhang Y, Wang Z, Liu C, Li W, et al. An efficient and benign antimicrobial depot based on silver-infused MoS₂. *ACS Nano*. 2017; 11: 4651-4659.
- Chernousova S, Epple M. Silver as antibacterial agent: ion, nanoparticle, and metal. *Angew Chem Int Ed*. 2013; 52: 1636-53.
- Barras A, Martin FA, Bande O, Baumann J-S, Ghigo J-M, Boukherroub R, et al. Glycan-functionalized diamond nanoparticles as potent *E. coli* anti-adhesives. *Nanoscale*. 2013; 5: 2307-16.
- Mukherjee S, Chowdhury D, Kotcherlakota R, Patra S. Potential theranostics application of bio-synthesized silver nanoparticles (4-in-1 system). *Theranostics*. 2014; 4: 316-35.
- Xiao S, Abu-Esba L, Turkyilmaz S, White AG, Smith BD. Multivalent dendritic molecules as broad spectrum bacteria agglutination agents. *Theranostics*. 2013; 3: 658-66.
- Cha S-H, Hong J, McGuffie M, Yeom B, VanEpps JS, Kotov NA. Shape-dependent biomimetic inhibition of enzyme by nanoparticles and their antibacterial activity. *ACS Nano*. 2015; 9: 9097-105.
- Applerot G, Lipovsky A, Dror R, Perkas N, Nitzan Y, Lubart R, et al. Enhanced antibacterial activity of nanocrystalline ZnO due to increased ROS-mediated cell injury. *Adv Funct Mater*. 2009; 19: 842-52.
- Sovadinova I, Palermo EF, Huang R, Thoma LM, Kuroda K. Mechanism of polymer-induced hemolysis: nanosized pore formation and osmotic lysis. *Biomacromolecules*. 2010; 12: 260-8.
- Wu Y, Long Y, Li Q-L, Han S, Ma J, Yang Y-W, et al. Layer-by-layer (LBL) self-assembled biohybrid nanomaterials for efficient antibacterial applications. *ACS Appl Mater Interfaces*. 2015; 7: 17255-63.
- Hancock RE, Sahl H-G. Antimicrobial and host-defense peptides as new anti-infective therapeutic strategies. *Nat Biotechnol*. 2006; 24: 1551-7.
- Marr AK, Gooderham WJ, Hancock RE. Antibacterial peptides for therapeutic use: obstacles and realistic outlook. *Curr Opin Pharmacol*. 2006; 6: 468-72.
- Jo Y-K, Kim BH, Jung G. Antifungal activity of silver ions and nanoparticles on phytopathogenic fungi. *Plant Dis*. 2009; 93: 1037-43.
- Bazzaz BSF, Khameneh B, Jalili-Behabadi M-m, Malaekheh-Nikouei B, Mohajeri SA. Preparation, characterization and antimicrobial study of a hydrogel (soft contact lens) material impregnated with silver nanoparticles. *Cont Lens Anterior Eye*. 2014; 37: 149-52.
- Richter AP, Brown JS, Bharti B, Wang A, Gangwal S, Houck K, et al. An environmentally benign antimicrobial nanoparticle based on a silver-infused lignin core. *Nat Nanotechnol*. 2015; 10: 817-23.
- De Jong WH, Van Der Ven LT, Sleijffers A, Park MV, Jansen EH, Van Loveren H, et al. Systemic and immunotoxicity of silver nanoparticles in an intravenous 28 days repeated dose toxicity study in rats. *Biomaterials*. 2013; 34: 8333-43.
- Li L, Sun J, Li X, Zhang Y, Wang Z, Wang C, et al. Controllable synthesis of monodispersed silver nanoparticles as standards for quantitative assessment of their cytotoxicity. *Biomaterials*. 2012; 33: 1714-21.
- Wilson BA, Salyers AA, Whitt DD, Winkler ME. Bacterial pathogenesis: a molecular approach: American Society for Microbiology (ASM); 2011.
- Allegranzi B, Nejad SB, Combescure C, Graafmans W, Attar H, Donaldson L, et al. Burden of endemic health-care-associated infection in developing countries: systematic review and meta-analysis. *Lancet*. 2011; 377: 228-41.
- Nugent RP, Krohn MA, Hillier SL. Reliability of diagnosing bacterial vaginosis is improved by a standardized method of gram stain interpretation. *J Clin Microbiol*. 1991; 29: 297-301.
- Oethinger M, Warner DK, Schindler SA, Kobayashi H, Bauer TW. Diagnosing periprosthetic infection: false-positive intraoperative Gram stains. *Clin Orthop Relat Res*. 2011; 469: 954-60.
- Grunow R, Spletstoesser W, McDonald S, Otterbein C, O'Brien T, Morgan C, et al. Detection of *Francisella tularensis* in biological specimens using a capture enzyme-linked immunosorbent assay, an immunochromatographic handheld assay, and a PCR. *Clin Diagn Lab Immunol*. 2000; 7: 86-90.
- Swanink C, Meis J, Rijs A, Donnelly JP, Verweij PE. Specificity of a sandwich enzyme-linked immunosorbent assay for detecting *Aspergillus galactomannan*. *J Clin Microbiol*. 1997; 35: 257-60.

38. Mothershed EA, Whitney AM. Nucleic acid-based methods for the detection of bacterial pathogens: present and future considerations for the clinical laboratory. *Clin Chim Acta*. 2006; 363: 206-20.
39. Muyzer G, De Waal EC, Uitterlinden AG. Profiling of complex microbial populations by denaturing gradient gel electrophoresis analysis of polymerase chain reaction-amplified genes coding for 16S rRNA. *Appl Environ Microb*. 1993; 59: 695-700.
40. Reller LB, Weinstein MP, Petti CA. Detection and identification of microorganisms by gene amplification and sequencing. *Clin Infect Dis*. 2007; 44: 1108-14.
41. Cheng D, Yu M, Fu F, Han W, Li G, Xie J, et al. Dual recognition strategy for specific and sensitive detection of bacteria using aptamer-coated magnetic beads and antibiotic-capped gold nanoclusters. *Anal Chem*. 2016; 88: 820-5.
42. Aw J, Widjaja F, Ding Y, Mu J, Liang Y, Xing BG. Enzyme-responsive reporter molecules for selective localization and fluorescence imaging of pathogenic biofilms. *Chem Commun*. 2017; 53: 3330-3.
43. Zeng W, Wang X, Xu P, Liu G, Eden HS, Chen X. Molecular imaging of apoptosis: from micro to macro. *Theranostics*. 2015; 5: 559-82.
44. Ning X, Lee S, Wang Z, Kim D, Stubblefield B, Gilbert E, et al. Maltodextrin-based imaging probes detect bacteria in vivo with high sensitivity and specificity. *Nat Mater*. 2011; 10: 602-7.
45. Zhang M, Zhu PP, Xin P, Si W, Li ZT, Hou JL. Synthetic channel specifically inserts into the lipid bilayer of Gram-positive bacteria but not that of mammalian erythrocytes. *Angew Chem Int Ed*. 2017; 56: 2999-3003.
46. Zhao E, Chen Y, Chen S, Deng H, Gui C, Leung CW, et al. A luminogen with aggregation-induced emission characteristics for wash-free bacterial imaging, high-throughput antibiotics screening and bacterial susceptibility evaluation. *Adv Mater*. 2015; 27: 4931-7.
47. Syal K, Mo M, Yu H, Iriya R, Jing W, Guodong S, et al. Current and emerging techniques for antibiotic susceptibility tests. *Theranostics*. 2017; 7: 1795-805.
48. Chung HJ, Reiner T, Budin G, Min C, Liong M, Issadore D, et al. Ubiquitous detection of gram-positive bacteria with bioorthogonal magnetofluorescent nanoparticles. *ACS Nano*. 2011; 5: 8834-41.
49. Zhong D, Zhuo Y, Feng Y, Yang X. Employing carbon dots modified with vancomycin for assaying Gram-positive bacteria like staphylococcus aureus. *Biosen Bioelectron*. 2015; 74: 546-53.
50. Van Oosten M, Schäfer T, Gazendam JA, Ohlsen K, Tsompanidou E, De Goffau MC, et al. Real-time in vivo imaging of invasive and biomaterial-associated bacterial infections using fluorescently labelled vancomycin. *Nat Commun*. 2013; 4: 2584-91.
51. Kohanski MA, DePristo MA, Collins JJ. Sublethal antibiotic treatment leads to multidrug resistance via radical-induced mutagenesis. *Mol Cell*. 2010; 37: 311-20.
52. Cavalieri F, Tortora M, Stringaro A, Colone M, Baldassarri L. Nanomedicines for antimicrobial interventions. *J Hosp Infect*. 2014; 88: 183-90.
53. Zhu X, Radovic-Moreno AF, Wu J, Langer R, Shi J. Nanomedicine in the management of microbial infection—overview and perspectives. *Nano Today*. 2014; 9: 478-98.
54. Li Q, Wu Y, Lu H, Wu X, Chen S, Song N, et al. Construction of supramolecular nanoassembly for responsive bacterial elimination and effective bacterial detection. *ACS Appl Mater Interfaces*. 2017; 9: 10180-89.
55. Wu MX, Wang X, Yang YW. Polymer nanoassembly as delivery systems and anti-bacterial toolbox: from PGMAs to MSN@ PGMAs. *Chem Rec*. 2017, DOI: 10.1002/tcr.201700036.
56. Beyth N, Hourri-Haddad Y, Domb A, Khan W, Hazan R. Alternative antimicrobial approach: nano-antimicrobial materials. *Evid Based Compl Alternat Med*. 2015; 2015: 246012-27.
57. Natan M, Banin E. From Nano to Micro: using nanotechnology to combat microorganisms and their multidrug resistance. *FEMS Microbiol Rev*. 2017; 41: 302-22.
58. Wang L, Hu C, Shao L. The antimicrobial activity of nanoparticles: present situation and prospects for the future. *Int J Nanomedicine*. 2017; 12: 1227-49.
59. Xie S, Manuguri S, Proietti G, Romson J, Fu Y, Inge A K, et al. Design and synthesis of theranostic antibiotic nanodrugs that display enhanced antibacterial activity and luminescence. *Proc Natl Acad Sci USA*. 2017; 114: 8464-9.
60. Hartgerink JD, Beniash E, Stupp SI. Self-assembly and mineralization of peptide-amphiphile nanofibers. *Science*. 2001; 294: 1684-8.
61. Bhattacharya S, Samanta SK. Soft-nanocomposites of nanoparticles and nanocarbons with supramolecular and polymer gels and their applications. *Chem Rev*. 2016; 116: 11967-2028.
62. Gao T, Yang S, Cao X, Dong J, Zhao N, Ge P, et al. A smart self-assembled organic nanoprobe for protein-specific detection: design, synthesis, application and mechanism studies. *Anal Chem*. 2017; 89: 10085-93.
63. Zhao Y, Thorkelsson K, Mastroianni AJ, Schilling T, Luther JM, Rancatore BJ, et al. Small-molecule-directed nanoparticle assembly towards stimuli-responsive nanocomposites. *Nat Mater*. 2009; 8: 979-85.
64. Ma Y, Mou Q, Sun M, Yu C, Li J, Huang X, et al. Cancer theranostic nanoparticles self-assembled from amphiphilic small molecules with equilibrium shift-induced renal clearance. *Theranostics*. 2016; 6: 1703-16.
65. Gao T, Cao X, Ge P, Dong J, Yang S, Xu H, et al. A self-assembled fluorescent organic nanoprobe and its application for sulfite detection in food samples and living systems. *Org Biomol Chem*. 2017; 15: 4375-82.
66. Gao T, Cao X, Dong J, Liu Y, Lv W, Li C, et al. A novel water soluble multifunctional fluorescent probe for highly sensitive and ultrafast detection of anionic surfactants and wash free imaging of Gram-positive bacteria strains. *Dyes Pigm*. 2017; 143: 436-43.
67. Zhao D, Zhao S, Zhao L, Zhang X, Wei P, Liu C, et al. Discovery of biphenyl imidazole derivatives as potent antifungal agents: design, synthesis, and structure-activity relationship studies. *Bioorg Med Chem*. 2017; 25: 750-8.
68. Anderson EB, Long TE. Imidazole-and imidazolium-containing polymers for biology and material science applications. *Polymer*. 2010; 51: 2447-54.
69. Riduan SN, Zhang Y. Imidazolium salts and their polymeric materials for biological applications. *Chem Soc Rev*. 2013; 42: 9055-70.
70. Jennings MC, Minbiole KP, Wuest WM. Quaternary ammonium compounds: an antimicrobial mainstay and platform for innovation to address bacterial resistance. *ACS Infect Dis*. 2015; 1: 288-303.
71. Zhang X, Chen X, Yang J, Jia H-R, Li Y-H, Chen Z, et al. Quaternized silicon nanoparticles with polarity-sensitive fluorescence for selectively imaging and killing gram-positive bacteria. *Adv Funct Mater*. 2016; 26: 5958-70.
72. Samby V, Peterson BR, Sen A. Antibacterial and hemolytic activities of pyridinium polymers as a function of the spatial relationship between the positive charge and the pendant alkyl tail. *Angew Chem Int Ed*. 2008; 47: 1250-4.
73. Yao Y, Chi X, Zhou Y, Huang F. A bola-type supra-amphiphile constructed from a water-soluble pillar [5] arene and a rod-coil molecule for dual fluorescent sensing. *Chem Sci*. 2014; 5: 2778-82.
74. Guan W, Zhou W, Lu C, Tang BZ. Synthesis and design of aggregation-induced emission surfactants: direct observation of micelle transitions and microemulsion droplets. *Angew Chem Int Ed*. 2015; 54: 15160-4.
75. Yuan H, Liu Z, Liu L, Lv F, Wang Y, Wang S. Cationic conjugated polymers for discrimination of microbial pathogens. *Adv Mater*. 2014; 26: 4333-8.
76. Bartholomew JW, Mittwer T. The gram stain. *Bacteriol Rev*. 1952; 16: 1-29.
77. Zhao Y, Tian Y, Cui Y, Liu W, Ma W, Jiang X. Small molecule-capped gold nanoparticles as potent antibacterial agents that target Gram-negative bacteria. *J Am Chem Soc*. 2010; 132: 12349-56.
78. Vaara M, Vaara T. Polycations as outer membrane-disorganizing agents. *Antimicrob Agents Chemother*. 1983; 24: 114-22.
79. Kadurugamuwa JL, Clarke AJ, Beveridge TJ. Surface action of gentamicin on *Pseudomonas aeruginosa*. *J Bacteriol*. 1993; 175: 5798-805.
80. Rizzello L, Cingolani R, Pompa PP. Nanotechnology tools for antibacterial materials. *Nanomedicine*. 2013; 8: 807-21.